Monitoring of Lung Stiffness for Long-COVID Patients Using Magnetic Resonance Elastography (MRE)

Sabine F Bensamoun, Kiaran P McGee, Mashhour Chakouch, Fabrice Charleux, Philippe Pouletaut

Monitoring of Lung Stiffness for Long-COVID Patients Using Magnetic Resonance Elastography (MRE)

Sabine F. Bensamoun[1], PhD, Kiaran P. McGee[2], PhD, Mashhour Chakouch[1], PhD, Philippe Pouletaut[1], PhD, Fabrice Charleux[3], MD

[1] Université de technologie de Compiègne, CNRS, BMBI (Biomechanics and Bioengineering), Compiègne, France

[2] Mayo Clinic & Foundation, Department of Radiology, Rochester, Minnesota, USA

[3] ACRIM-Polyclinique Saint Côme, Radiology department, Compiègne, France

Corresponding author:
Sabine F. Bensamoun
Université de technologie de Compiègne, Centre de recherche Royallieu, CS 60 319, 60 203 Compiègne Cedex, France
Tel: (33) 03 44 23 43 90
E-mail address: sabine.bensamoun@utc.fr

Declarations of interest: none

ABSTRACT

Purpose: Transaxial CT imaging is the main clinical imaging modality for the assessment of COVID-induced lung damage. However, this type of data does not quantify the functional properties of the lung. The objective is to provide non-invasive personalized cartographies of lung stiffness for long-COVID patients using MR elastography (MRE) and follow-up the evolution of this quantitative mapping over time.

Methods: Seven healthy and seven long-COVID participants underwent CT and MRE imaging at total lung capacity. After CT test, a senior radiologist visually analyzed the lung structure. Less than one month later, a first MRI (1.5 T, GRE sequence) lung density test followed by a first MRE (SE-EPI sequence) test were performed. Gadolinium-doped water phantom and a pneumatic driver (vibration frequency: 50 Hz), placed on the sternum, were used for MRI and MRE tests, respectively. Personalized cartographies of the stiffness were obtained, by two medical imaging engineers, using a specific post processing (MMDI algorithm). The monitoring (lung density, stiffness) was carried out no later than 11 months for each COVID patient. Wilcoxon's tests and an intra-class correlation coefficient (ICC) were used for statistical analysis.

Results: The density for long-COVID patients was significantly (P = 0.047) greater (170 $kg.m^{-3}$) compared to healthy (125 $kg.m^{-3}$) subjects. After the first MRE test, the stiffness measured for the healthy subjects was in the same range (median value (interquartile range, IQR): 0.93 (0.09) kPa), while the long-COVID patients showed a larger stiffness range (from 1.39 kPa to 2.05 kPa). After a minimum delay of 5 months, the second MRE test showed a decrease of stiffness (from 22 % to 40 %) for every long-COVID patient. The inter-operator agreement was excellent (intra-class correlation coefficient: 0.93 [0.78 - 0.97]).

Conclusion: The MRE test is sensitive enough to monitor disease-induced change in lung stiffness (increase with COVID symptoms and decrease with recovery). This non-invasive modality could yield complementary information as a new imaging biomarker to follow up long-COVID patients.

Keywords: computed tomography, long-COVID, lung density, lung, magnetic resonance elastography, lung stiffness

Abbreviations:

BMI, body mass index;

CT, computed tomography;

FOV, field of view;

ICC, intraclass correlation coefficient;

IQR, interquartile range;

MEG, motion-encoding gradient;

MRE, magnetic resonance elastography;

MRI, magnetic resonance imaging;

ROI, region of interest;

SD, standard deviation;

SE-EPI, spin-echo echo-planar imaging

1. Introduction

Patients infected by the 2019 coronavirus disease (COVID) are not all affected in the same way, and recovery can be either without after-effects, for example for asymptomatic people, or with more or less significant symptoms. The main symptoms include fatigue, headache, attention disorders, dyspnea [1], and may still be present 24 months after the COVID infection [2]. According to the World Health Organization [3], "post-COVID-19" or "long-COVID" condition occurs in individuals with a history of probable or confirmed SARS CoV-2 infection, usually 3 months from the onset of COVID-19 with symptoms and that last for at least 2 months and cannot be explained by an alternative diagnosis. Although the mechanisms are not fully understood, different therapies (chemical, physiotherapy, etc.) are prescribed [4-5] and the clinician needs to follow up the effect of the treatment.

In case of lung damage caused by the COVID, patients show varying degrees of respiratory difficulties (cough, shortness of breath) [6]. During the pandemic, different imaging techniques [7] (radiography, computed tomography (CT), ultrasound (US), magnetic resonance imaging (MRI)) were used to characterize the structural properties of the lung and evaluate the level of severity of the damage, in order to adapt the treatment. CT scan was the main medical test used to evaluate the features of the lung COVID, including ground class opacity, consolidation, crazy paving, reticulation [8-11]. Moreover, post treatment of CT images was driven by artificial intelligence to stage and predict the evolution of the lung disease [12-13]. CT COVID features were also compared to ultrasound (US) lung images which recently applied a deep neural network to analyze the US acquisitions [14]. It should be noted that B mode ultrasound images are rarely used for regular lung investigation due to the air-filled alveoli, which lead to artifacts caused by the reflection of the beam. During the pandemic, this technique was however helpful to explore the echogenic pattern of the subpleural region, which was modified depending on the stage of the infection [15].

In addition to the US technique, dynamic contrast enhanced [16] and hyperpolarised gas MR [17-18] showed utility in tracking patients with lung pathologies. Thus, MRI was also conducted on COVID patients [19], and Fields's study [20] demonstrated similar morphological and textural results compared to CT COVID analysis. While lung MRI is a challenging task due to the low signal noise ratio, this imaging modality allowed the identification of the inflammatory areas and fibrotic regions [21]. The main advantage of MRI and US tests compared to CT scans is that they do not involve exposure to ionization radiation. CT, US and MRI are imaging tools that provide anatomical and structural

information, but these techniques do not quantify the tissue functional properties, such as the stiffness.

In 1995, a non-invasive phase-contrast technique, called magnetic resonance elastography (MRE), based on the application of motion encoding gradients, was developed to quantify the stiffness of soft tissues [22]. Thus, the functional properties of healthy and pathological muscle [23-24], liver [25-26], brain [27-28] were measured. Developing a lung MRE test was a technical challenge due to the amount of air present in the parenchyma, which leads to a noisy signal of phase data [29]. In 2006, the technical feasibility was demonstrated by Goss's study (2006) [30]. In addition, Mariappan et al. (2011) [31] demonstrated the feasibility of using the MRE technique to quantify healthy lung stiffness at different respiratory states. The variation in stiffness was then analyzed according to the age and sex [32], as well as in patients with interstitial lung disease (ILD), showing an increase in stiffness compared to normal lungs [33]. The purpose of the present study is to provide personalized cartographies of lung stiffness for long-COVID patients using the MRE technique, and to follow up the evolution of this quantitative mapping over time.

2. Materials and Methods

2.1. Participants

All participants were recruited at the radiology department, named ACRIM, located at the Polyclinic Saint Côme (Compiègne, France). All the subjects had a medical order prescribed by the family physician for a lung CT test (cough, tobacco control, …). This study was approved by the Institutional Review Board of ILE DE FRANCE III (#2020-A01496-33). All subjects had the experimental protocol explained, a reflection period, and then gave their informed written consent prior to admission into the study. Exclusion criteria were the contraindications for MRI (such as pregnancy, claustrophobia, pacemakers), people under the age of 18 years, and without lung fibrosis such as the chronic obstructive pulmonary disease (COPD).

Healthy patients are defined as subjects with no history of lung disease and no pulmonary damage visible by the radiologist on the CT images. A long-COVID patient is defined as a patient having presented a COVID persistent infection (for at least three months) [13] certified by a positive RT-PCR (Reverse Transcriptase - Polymerase Chain Reaction) test. All selected participants are non-smokers, so that smoking does not influence the results.

Among the twelve long-COVID patients recruited, five were unable to return for the second MRE test due to their moving to another region (N=2), a hospitalization (N=1), and 2 not wanting to participate anymore. Thus, seven long-COVID patients were finally part of the study.

In summary (Table 1), seven healthy volunteers (median value (interquartile range (IQR)): age = 59 (9) years, body mass index (BMI) = 24 (7) $kg.m^{-2}$, 3 women and 4 men) and seven long-COVID patients (age = 55 (12) years, body mass index (BMI) = 27 (1) $kg.m^{-2}$, 7 women) referred for a lung CT scan, without injection of contrast product, were included in this study. All selected participants have approximately the same age, so that age does not influence the results. It should be noted that the long-COVID patients had a significant (P < 0.1) higher BMI compared to the healthy participants.

All healthy and long-COVID patients underwent a first MRE test (labeled MRE N°1) within one month of the CT exam (Table 1). Then, they returned at least 5 months later for a second MRE test (labeled MRE N°2) (Table 1) after checking that they all had a negative antigenic test.

2.2. Computed Tomography (CT) Scan

Healthy volunteers (N = 7) and long-COVID patients (N = 7) had a single CT scan test. Lung CT images have been acquired with a multi-row detector (General Electric Revolution Maxima) system. Patients were examined during a single breath-hold at total lung capacity and the following parameters were applied for the thoracic CT acquisition: field of view: 43 x 43 cm^2; matrix: 512 x 512; voxel size: 0.84 x 0.84 x 0.625 mm^3; slice thickness: 0.625 mm and 100 - 140 kV according to the patient's weight. A senior radiologist subjectively analyzed the texture and the structural properties (bronchial thickness, ground glass, presence of emphysema) of the image. Moreover, the slice level where the intermediate trunk was clover-shaped in appearance was identified (Fig. 1a-c) for future MRE assessment of the same lung region. CT density was calculated by converting the measured Hounsfield number into density units [34].

2.3. Lung Density

The measurement of the lung density (ρ) is an important step to accurately quantify the lung stiffness usually represented by the shear modulus ($\mu = \rho v^2$, v: velocity of the shear

wave propagation) [35]. MRE is mainly applied to soft tissues having a density closed to 1000 $kg.m^{-3}$ similarly to the water. However, the lung is mainly composed of air and the volume varies from patient to patient. Thus, it was necessary to acquire a map of lung density for each patient to obtain a personalized stiffness mapping.

This mapping was obtained from MRI (General Electric Signa Artist machine) acquisition performed at breath-hold (22 s), for 4 axial slices (Fig. 1b) determined from CT scan where the clover-shaped was identified, with a fast gradient echo (GRE) sequence [35] and a TR of 15 ms, from which the initial signal of the lung was estimated. The MRI acquisition was performed with the following parameters: field of view: 48 x 48 cm^2; voxel size: 7.5 × 7.5 × 15 mm^3; matrix: 64 x 64; slice thickness: 15 mm; and flip angle: 10°. Before running the MR density sequence, a gadolinium-doped water phantom was placed on the sternum (Fig. 1d) to have a calibration [36], and the density values were compared with the CT density measurements.

The lung density map was computed on the basis of three steps:

1) Image acquisition of MR signal at 8 echo times t_j (t_1=TE1=1.828 ms; t_2=TE2=1.028 ms; t_3=TE1; t_4=TE2; t_5=TE1; t_6=TE2; t_7=TE1; t_8=TE2) expressed by: $I_j = I_0 \exp(- t_j / T2^*)$ for the determination of the initial signal I_0 and the relaxation time $T2^*$ of the lung;

2) Calibration acquisition with gadolinium-doped water phantom for the determination of a correction factor (CF) from MR acquisition at two repetition times (TR) according to the study of Theilmann et al. [37]:

CF = (mean phantom signal at TR = 6 s) / (mean phantom signal at TR = 10 ms) (1)

3) Calculation of the lung density map (ρ):

$$\rho = \frac{I_0}{CF * I_{ph}} \quad (2)$$

where I_{ph} is the mean signal measured inside the region of interest of the gadolinium-doped water phantom, *CF* the correction factor, and I_0 the mean signal of the lung at an echo time of zero [37].

At the step 1, the MR sequence were acquired alternating between a long (TE1) and a short (TE2) echo time, repeated four times, to reduce the effect of noise and to optimize the signal to noise ratio as realized in Theilmann's study [37].

2.4. Magnetic Resonance Elastography (MRE)

MRE tests were launched, at breath-hold (22 s), a few minutes after the density acquisition. They were realized at the same slice level, determined by the radiologist from the CT scan, as for MRI density tests. Then, MRE acquisitions were performed using a 2D multi-shot spin-echo echo-planar imaging (SE-EPI) sequence on a 1.5 T General Electric Signa Artist machine with an echo train length value of 8. MRE measurements were performed at total lung capacity, with a 22 s breath-hold for the scan time. Then, a round pneumatic driver (Resoundant, Mayo Clinic Foundation, Rochester, MN, USA), currently used for MRE liver tests [38], was placed on the right lung in order to avoid the motion artifact of the heart (Fig. 2). This driver is connected to a plastic tube where air pressure is induced at a frequency of 50 Hz using an acoustic speaker system.

The MRE pulse sequence including a motion-encoding gradient, which oscillated in the Z direction, was used to image the displacement of the shear waves. The phase images were recorded with the following parameters: FOV: 48 × 48 cm^2; TR: 250 ms; slice thickness: 15 mm; number of axial slices: 4; voxel size: 3.75 × 3.75 × 15 mm^3; matrix: 128 x 128; 4 phase offsets.

The post-processing of the phase images (Fig. 3a) was performed by two engineer operators, having a medical imaging training, with more than ten years of experience in MRE field of research) to obtain the true lung stiffness map (Fig. 3d) by three successive steps: 1) a region of interest was drawn on the 4 phase images (Fig. 3a) to select only the right lung to avoid the heart motion, 2) the apparent lung stiffness (Fig. 3b) was calculated from the phase images, by using a multi-model direct inversion (MMDI), executed using MRElab software (Mayo Clinic, Rochester, Minnesota,USA), with a specific post processing method (phase unwrapping based on minimum discontinuity algorithm and spatial Butterworth filter from 4 to 40 waves / FOV) [39], and then 3) corrected by the product of the apparent stiffness with the density map (Fig. 3c). This product process was done with ImageJ software (version 1.48v; National Institutes of Health, Bethesda, MD, USA) and a homemade macro code.

2.5. Statistical Analysis

All the statistical analyses were performed with R software. Due to the small sample size only non-parametric two-sample Wilcoxon-Mann-Whitney's tests were used to compare: 1) lung stiffness in healthy subjects and long-COVID patients for MRE N°1 test, and 2) the lung density in healthy subjects and long-COVID patients (using CT or MR N°1 tests). Paired Wilcoxon's tests were used to compare lung density or stiffness in the MRE N°1 and MRE N°2 tests. In addition, validation of lung density measurement between the two modalities (CT vs. MR) was realized with a Spearman correlation analysis. The level of significance was set at $P < 0.1$ instead of $P < 0.05$ because of the small sample size.

The intra-class correlation coefficient (ICC) and a Bland-Altman test were used to assess the agreement between the two operators to obtain the MRE lung stiffness. Agreement was classified as poor (ICC = 0.00-0.20), fair to good (ICC = 0.40-0.75) or excellent (ICC > 0.75) [40]. The value of ICC refers to the degree of overlap between the ROIs drawn by the two operators for the four axial slices.

3. Results

3.1. CT Images and Density Measurements

While the patients underwent the CT tests at different times (between 3 and 37 months) after their last COVID infection (Table 1), all the CT images revealed a "normal" scanner image, with parenchyma tissue without any ground glass, emphysema, inflammation, fibrosis, etc. in the region where the MR density test N°1 was performed. The CT density measurements (from 134 to 204 $kg.m^{-3}$) were in the same range as the MR density test N°1 (from 155 to 212 $kg.m^{-3}$) for each subject (Table 2); no significant difference was observed between the two imaging modalities ($P = 0.225$). This result was confirmed by the Spearman test which provided a r coefficient of 0.505. Moreover, the correlation value was statistically significant ($P = 0.081$). This analysis validated the density map which will be used for the data post-processing to personalize the lung stiffness cartography for each patient.

Compared to MR densities measured for the healthy group (Table 1), the MR densities measured for the long-COVID patients in MR test N°1 were significantly greater (median value (IQR): 170 (26) $kg.m^{-3}$ vs 125 (36) $kg.m^{-3}$, $P = 0.047$). A similar increase was also observed with the CT modality (median value (IQR): 157 (26) $kg.m^{-3}$ vs 133 (36) $kg.m^{-3}$, $P = 0.086$).

The evolution of the MR lung density over time, i.e from MR test N°1 to MR test N°2 (Table 1), shows globally a non-significant decrease (median value (IQR): 170 (26) $kg.m^{-3}$ vs 154 (19) $kg.m^{-3}$, $P = 0.176$). It varies differently from one patient to another (Table 2). For instance, Figure 4 showed an important decrease (about 27 %) in lung density for patients #4, #5 and #7, a slight decrease (12.2 %) for patient #6, and a stable density over time for patients #1 and #2. Only patient #3 showed a slight increase (13.7 %) in lung density.

3.2. MRE Lung Stiffness

Figure 3b showed a uniform spatial distribution of the healthy apparent lung stiffness due to the implicit hypothesis of the uniform density fixed to 1000 $kg.m^{-3}$. However, Figure 3d showed the cartography of the healthy corrected lung stiffness, represented by the distribution of shades of blue in the different parts of the lung. The median (IQR) stiffness was 0.93 (0.09) kPa (Table 1), corresponding to a range between 0.71 kPa and 1.01 kPa. A smaller range of stiffness was obtained for the healthy lung compared to the long-COVID patients showing a larger distribution of stiffness (from 1.39 to 2.12 kPa) indicating an inhomogeneous lung media. It can be noted that patient #7, at MR test N°1, showed the highest MR density (Fig.4, Table 2), which could be a characteristic of the pneumonia caused by COVID, inducing the increase of the corrected stiffness value (Fig.5, Table 3). Concerning the long-COVID patients, the MR stiffness measured in MR test N°1 was significantly greater than that measured for the healthy group (median value (IQR): 1.93 (0.46) kPa vs 0.93 (0.09) kPa, $P = 0.002$). These results were consistent with the increase in wavelength observed on the phase image for the long-COVID patients compared to the healthy subjects.

After the first MRE test, all the cartographies showed a diffuse distribution of color (Fig. 5) within the lung, indicating a variation in stiffness.

Interestingly, the second MRE test, performed at least 4 months later, showed a decrease (from 22 % to 40 %) in the personalized mean stiffness values (Fig. 6, Table 3) for each patient. However, patient #2 had the same stiffness value (1.6 kPa) even 9 months after the first MRE test. In the seven long-COVID patients, significant stiffness differences were observed between the first and the second MRE test ($P = 0.027$).

The post processing of the stiffness measurement was carried out by two different operators skilled in medical image analysis. The results of the intraclass correlation coefficient (ICC) and 95 % limits-of-agreement showed an excellent (0.93 [0.78- 0.97]) inter-

operator agreement for the lung stiffness measurement. In addition, the Bland-Altman plot (Fig. 7) showed also the agreement between the two operators: average difference of stiffnesses between the two operators was 0.0275 kPa. The 95% lower and upper limits of agreement were: - 0.1733 kPa and 0.2284 kPa.

4. Discussion

People react to a virus in different ways, with symptoms that can last different amounts of time. In the present study, patients had lung COVID symptoms (such as cough, dyspnea) which were still present a few months after the infection. CT tests, which provide an excellent image resolution (about 0.8 mm), did not reveal any morphological or structural abnormalities, visually detected by the radiologist, in any of the long-COVID patients who complained of lung discomfort. However, the density parameter measured for long-COVID patients showed a significant increase in comparison with the density for the healthy subjects. This may explain the long-COVID symptoms in the patients of our study. Nevertheless, the measurement of the CT density is rarely made in clinical practice, except for the analysis of pulmonary nodules or tumors. Moreover, density is not an appropriate parameter to characterize the functional properties of lung tissue. Thus, the first objective was to provide an additional quantitative parameter, i.e. lung stiffness, to evaluate the dynamic properties of the parenchyma.

Interestingly, after the first MRE test, all the long-COVID patients had a higher stiffness compared to the healthy control volunteers. It should be noted that the measurement of the healthy stiffness was in agreement with the literature for healthy MRE lungs [32]. The increase in stiffness indicates that the lung tissue is less deformable, leading to respiratory inconsistencies. Similar variations in stiffness were found in other MRE studies analyzing pathological lungs, such as those observed in patients with cystic fibrosis [36] or interstitial lung disease (ILD) [33]. In general, in the case of lung disease, CT scans showed structural variations. Thus, the first originality of the present study was to demonstrate that, even though CT scans showed no structural lung abnormalities for long-COVID patients, MRE tests could yield complementary information with a new biomarker of stiffness, which may explain the symptoms experienced by the patients. It would have been interesting to analyze the variations in stiffness according to the presence of ground glass opacities or other features caused by COVID. However, due to the delay in obtaining the ethical authorization, this study was carried out after the COVID pandemic.

Longitudinal follow-up is difficult with CT scans due to several factors, such as the stochastic and determinist effects [41] induced by exposure to ionization radiation, the variable swelling of the patient's pulmonary tissue which can create inconsistencies, etc. The second originality of the present study was to follow up long-COVID patients with the MRE technique. This is the first lung monitoring study showing the sensitivity of the MRE technique to reveal variations in stiffness over time. Indeed, all of the personalized cartography, except for one patient who still presented bronchia sequelae, showed a decrease in stiffness in the different parts of the lung. In addition, two patients (#1 and #3) made a full recovery demonstrated by a cartography showing a homogeneous distribution of stiffness. The present study has demonstrated the capability and the sensitivity of the MRE technique for the monitoring of lung parenchyma. Moreover, the accuracy of the MRE lung stiffness measurement was shown by the excellent Intraclass Correlation Coefficient result.

The third originality was the comparison of the density values with two imaging modalities (CT vs MRI), validating the present MR density values. Nevertheless, no direct correlation was made between the MR density and the stiffness values over time. Indeed, three patients (#1, #2, #3) showed opposite variations in stiffness and density over time. The relationship between density and stiffness needs further investigation with a higher number of patients.

The present study had several limitations, such as not using the pulmonary function test (PFT) which is mainly performed by a pneumologist to evaluate the level of fibrosis. In the present study, COPD patients were not included and most of the patients were referred by their family physician which does not perform PFT test. It would be interesting to simultaneously analyze the PFT and stiffness results. Moreover, different respiration phases and the depth of breathing could be performed to analyze the influence of the pre-strained condition of the tissue on the stiffness data. Also, the MRE set-up could be improved to analyze both lungs and the effect of sex on long-COVID lung stiffness. In the present study, the round pneumatic liver driver, which is available in clinical centers, was used for clinical practical purposes. However, a recent flexible pneumatic driver, with a long rectangular shape, also produced by Resoundant company, could be placed in the sternum to analyze simultaneously the stiffness of both lungs. In complement to the set-up, the time of MRE phase image acquisition could be reduced with the recording of only one axial slice of the lung instead of the four slices prescribed in this study, to reduce the breath-hold time during the test.

5. Conclusions

CT tests are customarily used for lung investigation, but the diagnosis is often dependent on the experience of the radiologist, with increased inter and intra-operator variability [12]. MRE tests could provide a measure of lung stiffness as a quantitative biomarker, in addition to the subjective information (texture, structure, visual score acquisitions) provided by CT tests. The present study demonstrates that MRE tests could be used as a minimally invasive imaging modality, avoiding exposure to ionization radiation, which could be an alternative to CT tests for the follow-up of lung tissue. This method paves the way for other lung applications.

Acknowledgments

We wish to thank Dr. Ehman, MRE department, Mayo Clinic & Foundation, Rochester, Minnesota, USA for MRE support.

Funding

This project was co-founded by the European Union through the European Regional Development Fund (FEDER/ERDF) within the framework of the Contrat de Plan Etat-Région (CPER) tecsante 2021-2027 for the Hauts-de-France region.

References

1. Lopez-Leon S, Wegman-Ostrosky T, Perelman C, et al. More than 50 long-term effects of COVID: a systematic review and meta-analysis. Sci Rep. 2021;11(1):1-12. doi:10.1038/s41598-021-95565-8

2. Kim Y, Bae S, Chang HH, Kim SW. Characteristics of long COVID and the impact of COVID vaccination on long COVID 2 years following COVID infection: prospective cohort study. Sci Rep. 2024;14(1):854. doi:10.1038/s41598-023-50024-4

3. World Health Organization. Post COVID-19 condition (Long COVID). Available at: https://www.who.int/srilanka/news/detail/16-10-2021-post-covid-19-condition . Accessed July 6th 2024.

4. Gheorghita R, Soldanescu I, Lobiuc A, et al. The knowns and unknowns of long-COVID: from mechanisms to therapeutical approaches. Front Immunol. 2024;15. doi:10.3389/fimmu.2024.1344086

5. Myall KJ, Mukherjee B, Castanheira AM, et al. Persistent Post-COVID Interstitial Lung Disease. An Observational Study of Corticosteroid Treatment. Annals ATS. 2021;18(5):799-806. doi:10.1513/AnnalsATS.202008-1002OC

6. Christopher DJ, Isaac BTJ, John FB, et al. Impact of post-COVID lung damage on pulmonary function, exercise tolerance and quality of life in Indian subjects. PLOS Global Public Health. 2024;4(2):e0002884. doi:10.1371/journal.pgph.0002884

7. Dong D, Tang Z, Wang S, et al. The Role of Imaging in the Detection and Management of COVID: A Review. IEEE Reviews in Biomedical Engineering. 2021;14:16-29. doi:10.1109/RBME.2020.2990959

8. Kanne JP. Chest CT Findings in 2019 Novel Coronavirus (2019-nCoV) Infections from Wuhan, China: Key Points for the Radiologist. Radiology. Published online February 4, 2020. doi:10.1148/radiol.2020200241

9. Shi H, Han X, Zheng C. Evolution of CT Manifestations in a Patient Recovered from 2019 Novel Coronavirus (2019-nCoV) Pneumonia in Wuhan, China. Radiology. Published online February 7, 2020. doi:10.1148/radiol.2020200269

10. Hani C, Trieu NH, Saab I, et al. COVID pneumonia: A review of typical CT findings and differential diagnosis. Diagnostic and Interventional Imaging. 2020;101(5):263-268. doi:10.1016/j.diii.2020.03.014

11. Torkian P, Ramezani N, Kiani P, et al. Common CT Findings of Novel Coronavirus Disease 2019 (COVID): A Case Series. Cureus. 2020;12(3). doi:10.7759/cureus.7434

12. Chassagnon G, Vakalopoulou M, Battistella E, et al. AI-driven quantification, staging and outcome prediction of COVID pneumonia. Medical Image Analysis. 2021;67:101860. doi:10.1016/j.media.2020.101860

13. Cau R, Faa G, Nardi V, et al. Long-COVID diagnosis: From diagnostic to advanced AI-driven models. European Journal of Radiology. 2022;148. doi:10.1016/j.ejrad.2022.110164

14. Zhao L, Fong TC, Bell MAL. Detection of COVID-19 features in lung ultrasound images using deep neural networks. Commun Med. 2024;4(1):1-10. doi:10.1038/s43856-024-00463-5

15. Soldati G, Smargiassi A, Inchingolo R, et al. Is There a Role for Lung Ultrasound During the COVID Pandemic? Journal of Ultrasound in Medicine. 2020;39(7):1459-1462. doi:10.1002/jum.15284

16. Srinivas RK, Garg M, Debi U, Prabhakar N, Dhooria S, Agarwal R, et al. Evaluation of Dynamic Contrast-Enhanced and Oxygen-Enhanced Functional Lung Magnetic Resonance Imaging in Chronic Obstructive Pulmonary Disease Patients. Diagnostics. 2023;13(23): 3511. doi: 10.3390/diagnostics13233511

17. Zhang X, Angelini ED, Haghpanah FS, Laine AF, Sun Y, Hiura GT, et al. Quantification of lung ventilation defects on hyperpolarized MRI: The Multi-Ethnic Study of Atherosclerosis (MESA) COPD study. Magnetic resonance imaging. 2022;92:140-149. doi:10.1016/j.mri.2022.06.016

18. Kirby M, Heydarian M, Svenningsen S, Wheatley A, McCormack DG, Etemad-Rezai R, et al. Hyperpolarized ^{3}He magnetic resonance functional imaging semiautomated segmentation. Academic radiology. 2012;19(2):141-152. doi: 10.1016/j.acra.2011.10.007

19. Ates OF, Taydas O, Dheir H. Thorax Magnetic Resonance Imaging Findings in Patients with Coronavirus Disease (COVID). Academic Radiology. 2020;27(10):1373-1378. doi:10.1016/j.acra.2020.08.009

20. Fields BKK, Demirjian NL, Dadgar H, Gholamrezanezhad A. Imaging of COVID: CT, MRI, and PET. Seminars in Nuclear Medicine. 2021;51(4):312-320. doi:10.1053/j.semnuclmed.2020.11.003

21. Lonzetti L, Zanon M, Pacini GS, et al. Magnetic resonance imaging of interstitial lung diseases: A state-of-the-art review. Respiratory Medicine. 2019;155:79-85. doi:10.1016/j.rmed.2019.07.006

22. Muthupillai R, Lomas DJ, Rossman PJ, Greenleaf JF, Manduca A, Ehman RL. Magnetic Resonance Elastography by Direct Visualization of Propagating Acoustic Strain Waves. Science. 1995;269(5232):1854-1857. doi:10.1126/science.7569924

23. Chakouch MK, Pouletaut P, Charleux F, Bensamoun SF. Viscoelastic shear properties of in vivo thigh muscles measured by MR elastography. Journal of Magnetic Resonance Imaging. 2016;43(6):1423-1433. doi:10.1002/jmri.25105

24. Bensamoun SF, Charleux F, Debernard L, Themar-Noel C, Voit T. Elastic properties of skeletal muscle and subcutaneous tissues in Duchenne muscular dystrophy by magnetic resonance elastography (MRE): A feasibility study. IRBM. 2015;36(1):4-9. doi:10.1016/j.irbm.2014.11.002

25. Leclerc GE, Charleux F, Robert L, et al. Analysis of liver viscosity behavior as a function of multifrequency magnetic resonance elastography (MMRE) postprocessing. Journal of Magnetic Resonance Imaging. 2013;38(2):422-428. doi:10.1002/jmri.23986

26. Bensamoun SF, Leclerc GE, Debernard L, et al. Cutoff Values for Alcoholic Liver

Fibrosis Using Magnetic Resonance Elastography Technique. Alcoholism: Clinical and Experimental Research. 2013;37(5):811-817. doi:10.1111/acer.12025

27. Green MA, Bilston LE, Sinkus R. In vivo brain viscoelastic properties measured by magnetic resonance elastography. NMR in Biomedicine. 2008;21(7):755-764. doi:10.1002/nbm.1254

28. Murphy MC, Huston J, Ehman RL. MR elastography of the brain and its application in neurological diseases. NeuroImage. 2019;187:176-183. doi:10.1016/j.neuroimage.2017.10.008

29. Chakouch M, Charleux F, Pouletaut P, Bensamoun S. MR elastography of the human lung. State of the Art in Bioengineering. 2022;2(1). Accessed July 6th, 2024. https://hal.science/hal-03562216

30. Goss B c., McGee K p., Ehman E c., Manduca A, Ehman R l. Magnetic resonance elastography of the lung: Technical feasibility. Magnetic Resonance in Medicine. 2006;56(5):1060-1066. doi:10.1002/mrm.21053

31. Mariappan YK, Glaser KJ, Hubmayr RD, Manduca A, Ehman RL, McGee KP. MR elastography of human lung parenchyma: Technical development, theoretical modeling and in vivo validation. Journal of Magnetic Resonance Imaging. 2011;33(6):1351-1361. doi:10.1002/jmri.22550

32. Fakhouri F, Kannengiesser S, Pfeuffer J, Gokun Y, Kolipaka A. Free-breathing MR elastography of the lungs: An in vivo study. Magnetic Resonance in Medicine. 2022;87(1):236-248. doi:10.1002/mrm.28986

33. Marinelli JP, Levin DL, Vassallo R, et al. Quantitative assessment of lung stiffness in patients with interstitial lung disease using MR elastography. Journal of Magnetic Resonance Imaging. 2017;46(2):365-374. doi:10.1002/jmri.25579

34. Schneider U, Pedroni E, Lomax A. The calibration of CT Hounsfield units for radiotherapy treatment planning. Phys Med Biol. 1996;41(1):111. doi:10.1088/0031-9155/41/1/009

35. Holverda S, Theilmann RJ, Sá RC, et al. Measuring lung water: Ex vivo validation of multi-image gradient echo MRI. Journal of Magnetic Resonance Imaging. 2011;34(1):220-224. doi:10.1002/jmri.22600

36. Cho Y, Fakhouri F, Ballinger MN, et al. Magnetic Resonance Elastography and Computational Modeling Identify Heterogeneous Lung Biomechanical Properties during Cystic Fibrosis. Published online March 21, 2024. doi:10.21203/rs.3.rs-4125891/v1

37. Theilmann RJ, Arai TJ, Samiee A, et al. Quantitative MRI measurement of lung density must account for the change in T with lung inflation. *Journal of Magnetic Resonance Imaging*. 2009;30(3):527-534. doi:10.1002/jmri.21866

38. Pouletaut P, Boussida S, Ternifi R, et al. Impact of Hepatic Iron Overload in the Evaluation of Steatosis and Fibrosis in Patients with Nonalcoholic Fatty Liver Disease Using Vibration-Controlled Transient Elastography (VCTE) and MR Imaging Techniques: A Clinical Study. IRBM. 2023;44(3):100750.

doi:10.1016/j.irbm.2022.100750

39. Silva AM, Grimm RC, Glaser KJ, et al. Magnetic resonance elastography: evaluation of new inversion algorithm and quantitative analysis method. Abdom Imaging. 2015;40(4):810-817. doi:10.1007/s00261-015-0372-5

40. Fleiss JL, Levin B, Paik MC. The Measurement of Interrater Agreement. In: Statistical Methods for Rates and Proportions. John Wiley & Sons, Ltd; 2003:598-626. doi:10.1002/0471445428.ch18

41. Brower C, & Rehani MM. Radiation risk issues in recurrent imaging. The British journal of radiology. 2021;94(1126), 20210389. doi: 10.1259/bjr.20210389

Tables

Table 1. Characteristics of the healthy and long-COVID patients

Patient group	**Healthy**	**Long-COVID**
Number of patients	7	7
Age, median [IQR] (y)	59 (9)	55 (12)
BMI, median [IQR] ($kg.m^{-2}$)	24 (7)	27 (1)*
Delay between the last COVID infection and MRE N°1 test median [IQR] (months) (min-max) (months)	 - -	 15 (13) (3-37)
Delay between MRE N°1 test & CT test median [IQR] (days) (min-max) (days)	 20 (14) (6-33)	 11 (10) (4-16)
Delay between MRE N°1 & MRE N°2 median [IQR] (months) (min-max) (months)	 - -	 9 (2) (5-11)
CT lung density, median (IQR) ($kg.m^{-3}$)	133 (36)	157 (26)*
MR lung density, median (IQR) ($kg.m^{-3}$) MR N°1 MR N°2	 125 (36) -	 170 (26)* 154 (19)
Lung stiffness, median (IQR) (kPa) MRE N°1 MRE N°2	 0.93 (0.09) -	 1.93 (0.46)** 1.52 (0.41)*

BMI = body mass index; CT = computerized tomography; IQR = interquartile range; MRE = magnetic resonance elastography.

* and ** indicate the mean difference is significantly different at $P < 0.1$ and $P < 0.01$ (non-parametric paired Wilcoxon's test for comparison between MRE N°1 and N°2 tests and two-sample Wilcoxon-Mann-Whitney's test for the other comparisons).

- Indicates no measure was recorded.

Table 2. Lung density of the long-COVID patients measured with each test (CT, MR test N°1, MR test N°2) and delays between the tests

Patient	CT density mean ± sd ($kg.m^{-3}$)	MR test N°1 density mean ± sd ($kg.\ m^{-3}$)	MR test N°2 density mean ± sd ($kg.\ m^{-3}$)	MR density variation (%)	Delay CT – MR test N°1 (days)	MR Delay N°1-N°2 tests (months)
#1	134.3 ± 19.1	158.1 ± 105.4	170.9 ± 66.6	8.0	15	4.7
#2	186.5 ± 21.1	163.7 ± 62.5	159.0 ± 77.8	-2.9	6	9.1
#3	204.7 ± 22.0	155.2 ± 88.4	176.4 ± 41.8	13.7	11	10.1
#4	150.5 ± 20.9	175.8 ± 115.3	126.5 ± 49.8	-28.1	4	7.7
#5	167.1 ± 21.6	197.9 ± 177.2	153.8 ± 42.6	-22.3	16	10.3
#6	156.7 ± 21.5	169.6 ± 55.4	148.9 ± 50.5	-12.2	14	8.0
#7	151.1 ± 21.1	212.4 ± 93.9	144.1 ± 53.9	-32.2	4	11.2

CT = computerized tomography; MR = magnetic resonance; sd = standard deviation.

Table 3. Lung stiffness of the long-COVID patients measured for both MRE tests, and delay between MRE tests

Patient	MRE test N°1 stiffness mean ± sd (kPa)	MRE test N°2 stiffness mean ± sd (kPa)	Stiffness variation (%)	MRE delay N°1-N°2 tests (months)
#1	1.39 ± 1.06	1.00 ± 0.36	-28.1	4.7
#2	1.53 ± 0.60	1.65 ± 0.79	7.8	9.1
#3	1.54 ± 0.86	0.92 ± 0.33	-40.2	10.1
#4	1.93 ± 0.90	1.41 ± 0.55	-27.0	7.7
#5	1.95 ± 1.37	1.52 ± 0.41	-21.9	10.3
#6	2.05 ± 0.62	1.60 ± 0.58	-21.7	8.0
#7	2.12 ± 0.95	1.62 ± 0.65	-23.4	11.2

MRE = magnetic resonance elastography; sd = standard deviation.

Figure Legends

Fig. 1. Positioning of the four axial slices (red line) in coronal view with CT (a) and MR (b) acquisitions, in median axial slice with CT (c), and in one of the four axial MR (d) acquisitions with the gadolinium (Gd) phantom.

Fig. 2. MR elastography lung set up.

Fig. 3. Representation of the different steps for the post processing of the 4 phase images, acquired on a healthy subject, to obtain a personalized cartography of the right lung stiffness in the manually drawn region of interest (white dashed border).

Fig. 4. Evolution of the MR density values (mean and standard deviation) in the MR test N°1 and MR test N°2 for the 7 long-COVID patients.

Fig. 5. Personalized lung stiffness for the 7 long-COVID patients in the first and second MRE tests.

Fig. 6. Evolution of the lung stiffness values (mean and standard deviation) in the MRE test N°1 and MRE test N°2 for the 7 long-COVID patients.

Fig. 7. Bland-Altman plot of the lung stiffness obtained from 7 long-COVID patients analyzed by two operators.

Fig. 1

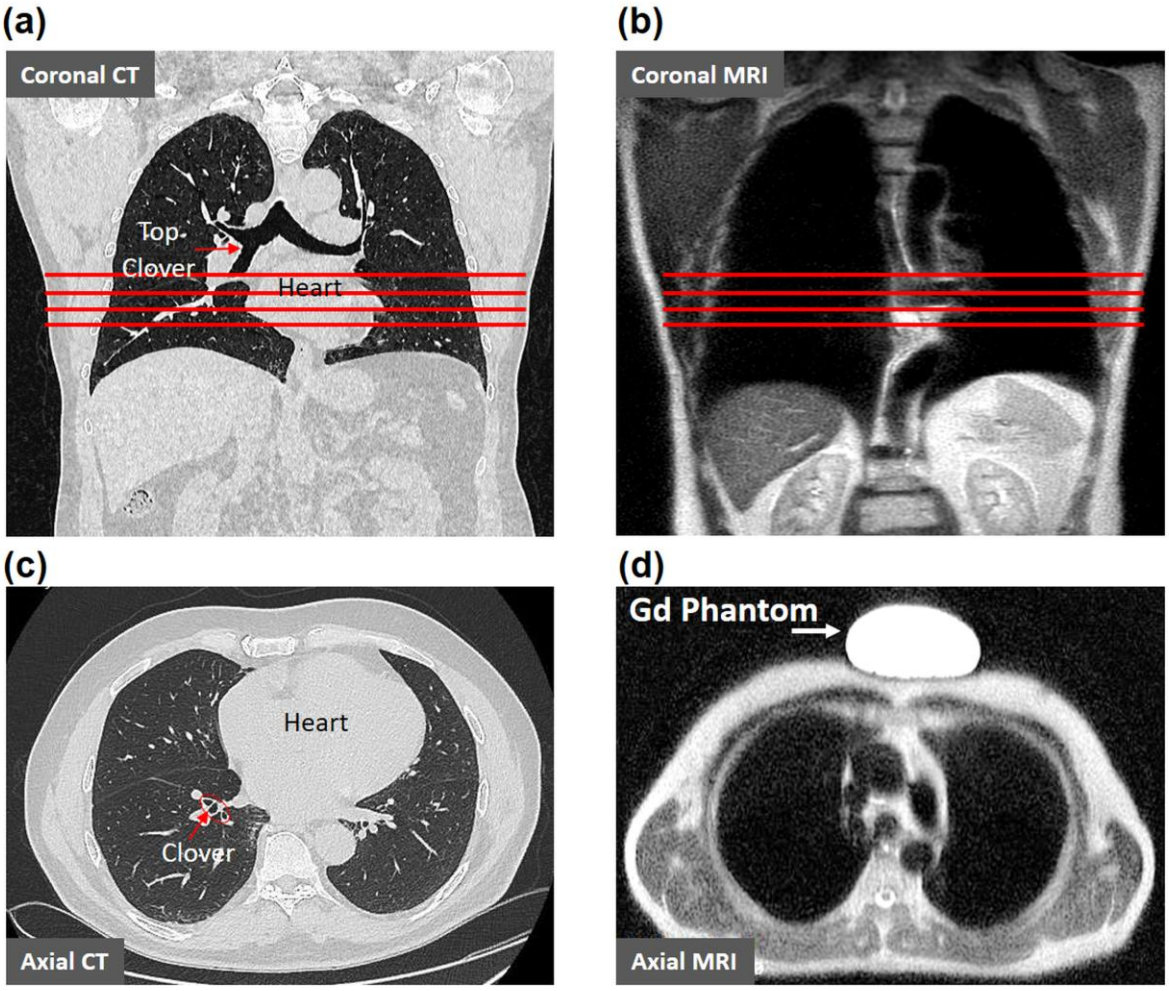
(a)
Coronal CT
Top
Clover
Heart
(b)
Coronal MRI
(c)
Heart
Clover
Axial CT
(d)
Gd Phantom
Axial MRI

Fig. 2

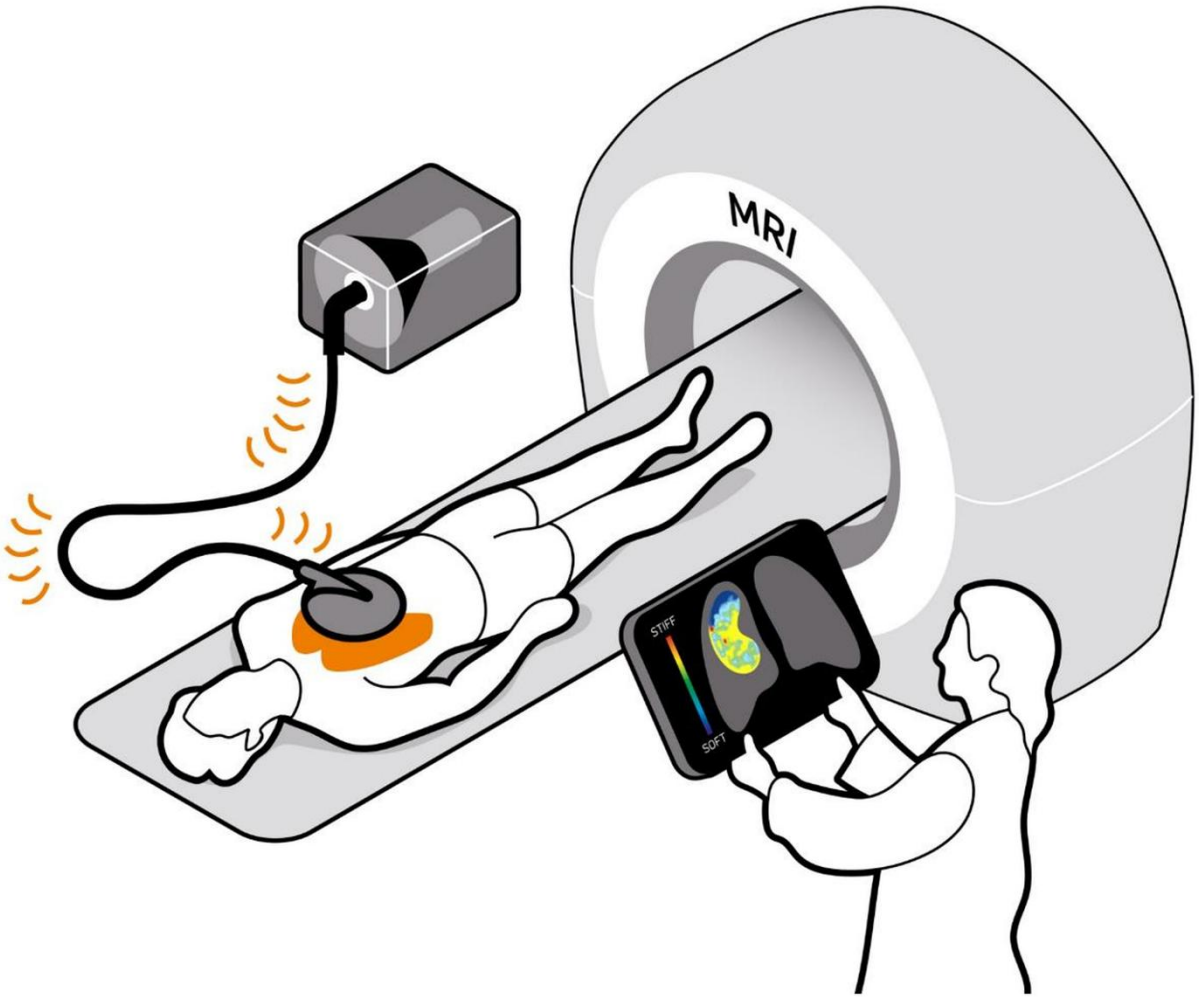

Fig. 3

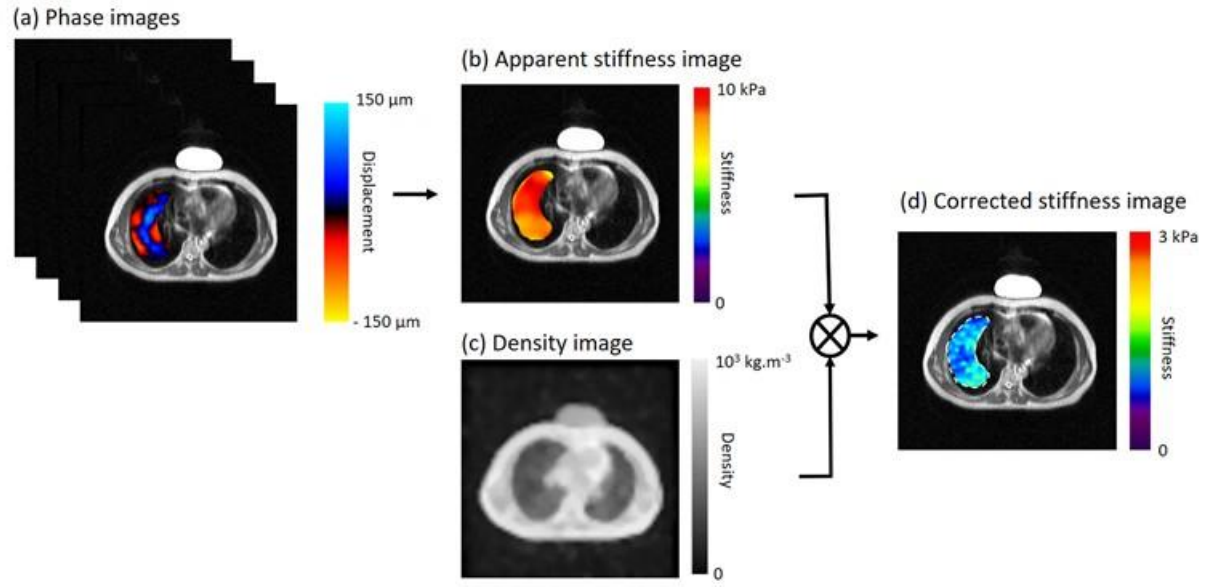
(a) Phase images
150 µm
Displacement
- 150 µm
(b) Apparent stiffness image
10 kPa
Stiffness
0
(c) Density image
10³ kg.m⁻³
Density
0
(d) Corrected stiffness image
3 kPa
Stiffness
0

Fig. 4

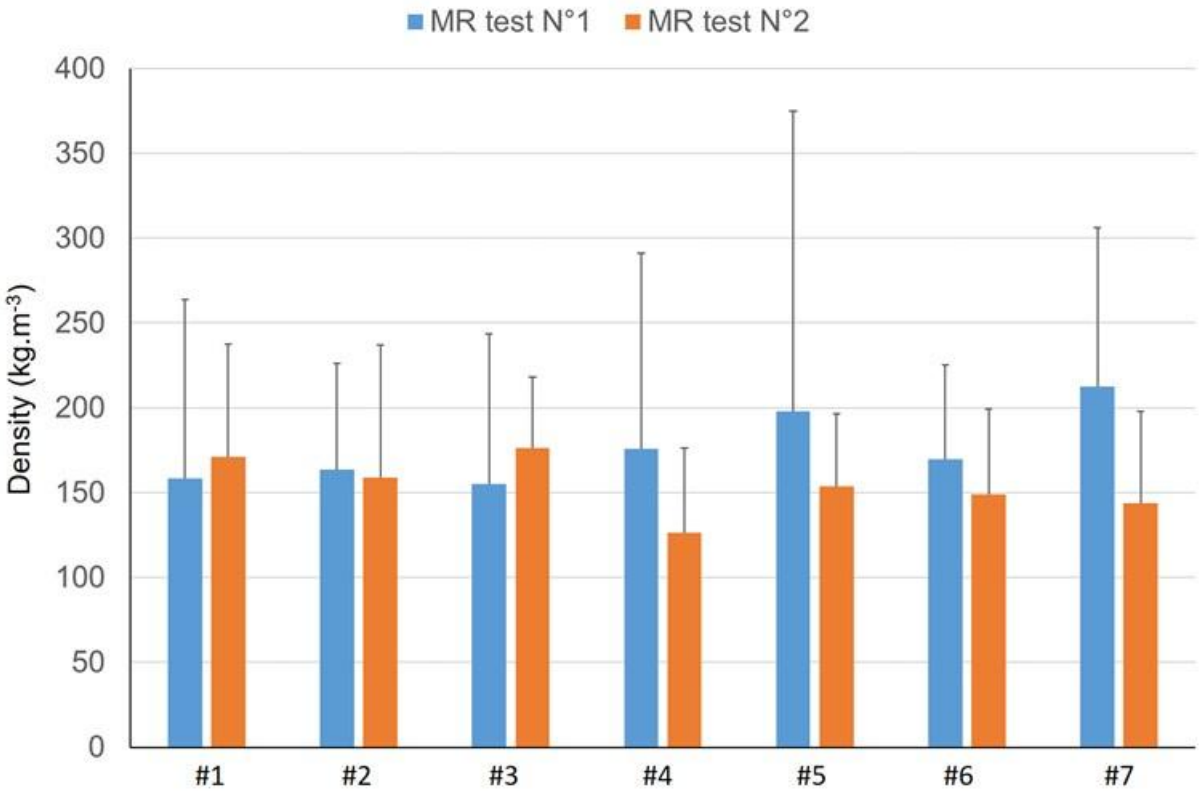
MR test N°1
MR test N°2
Density (kg.m-3)
400
350
300
250
200
150
100
50
0
#1
#2
#3
#4
#5
#6
#7

Fig. 5

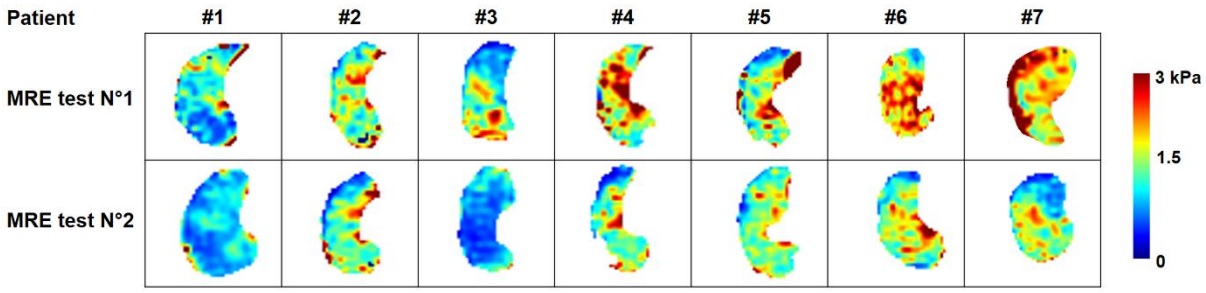

Fig. 6

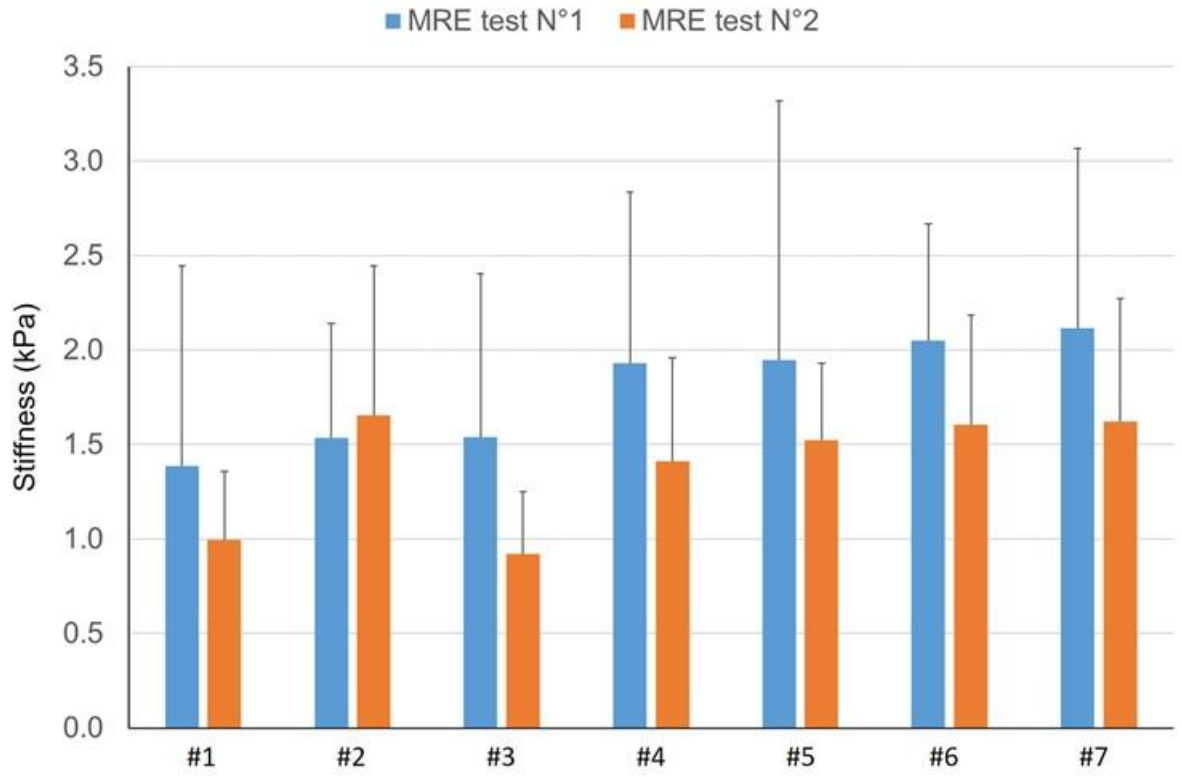
MRE test N°1
MRE test N°2
Stiffness (kPa)
3.5
3.0
2.5
2.0
1.5
1.0
0.5
0.0
#1
#2
#3
#4
#5
#6
#7

Fig. 7

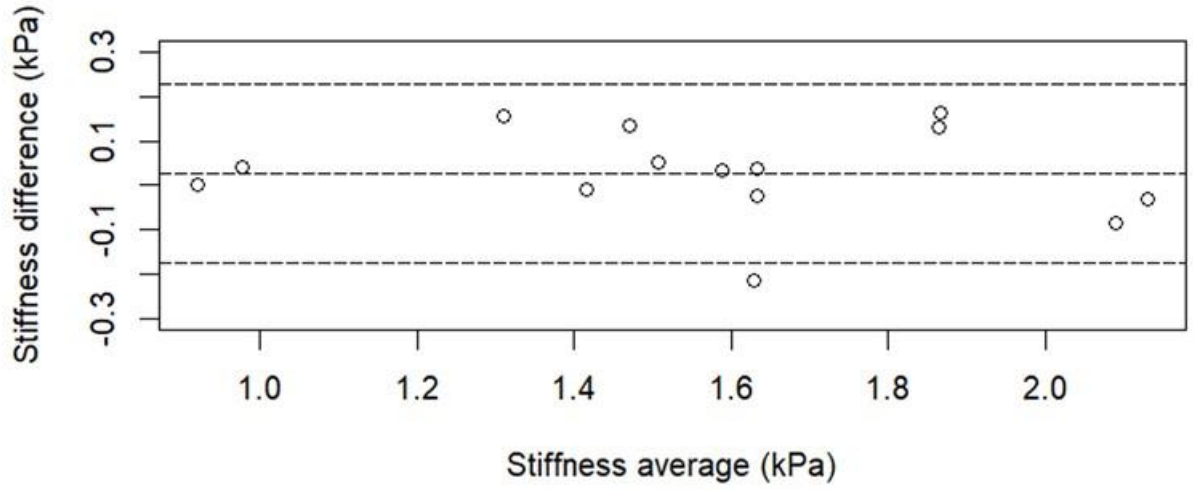
Stiffness difference (kPa)
0.3
0.1
-0.1
-0.3
1.0
1.2
1.4
1.6
1.8
2.0
Stiffness average (kPa)